nature energy

ARTICLES

PUBLISHED: 25 JANUARY 2016 | ARTICLE NUMBER: 15027 | DOI: 10.1038/NENERGY.2015.27

Efficient organic solar cells processed from hydrocarbon solvents

Jingbo Zhao[1†], Yunke Li[1†], Guofang Yang[1,2], Kui Jiang[1,3], Haoran Lin[1], Harald Ade[4], Wei Ma[2*] and He Yan[1,3*]

Organic solar cells have desirable properties, including low cost of materials, high-throughput roll-to-roll production, mechanical flexibility and light weight. However, all top-performance devices are at present processed using halogenated solvents, which are environmentally hazardous and would thus require expensive mitigation to contain the hazards. Attempts to process organic solar cells from non-halogenated solvents lead to inferior performance. Overcoming this hurdle, here we present a hydrocarbon-based processing system that is not only more environmentally friendly but also yields cells with power conversion efficiencies of up to 11.7%. Our processing system incorporates the synergistic effects of a hydrocarbon solvent, a novel additive, a suitable choice of polymer side chain, and strong temperature-dependent aggregation of the donor polymer. Our results not only demonstrate a method of producing active layers of organic solar cells in an environmentally friendly way, but also provide important scientific insights that will facilitate further improvement of the morphology and performance of organic solar cells.

Organic solar cell (OSC) technology is considered one of the most promising cost-effective and environmentally friendly solar cell technologies, as it can be produced using low-cost printing processes and the end product contains no toxic materials[1–9]. One of the major problems holding back the widespread use of OSCs is that all high-efficiency (>10%) devices are at present processed from hazardous halogenated solvents such as chlorobenzene (CB), 1,2-dichlorobenzene and additives such as 1,8-diiodooctane (DIO; refs 10–14). These solvents are harmful to people and the environment, and current state-of-the-art OSCs are thus not truly environmentally friendly in their production processes. In addition, halogenated solvents do not exist in nature, and their production requires relatively costly synthetic steps. Hydrocarbons are better choices of solvents for OSC production, as they are more environmentally friendly and readily available from petroleum. However, several reports have indicated that OSCs processed from non-chlorinated solvents generally result in significantly reduced power conversion efficiency (PCE) levels[15–22], and that the best OSCs are still processed from halogenated solvents[10–14]. One reason for the much poorer performance is that state-of-the-art donor and/or acceptor materials for OSCs typically exhibit poor solubility in non-halogenated solvents, which results in a poor bulk-heterojunction (BHJ) morphology containing excessively large domains[15]. On the other hand, controlling and optimizing BHJ morphology is one of the most important challenges for OSCs (ref. 23). Some morphology parameters (for example, molecular orientation at or relative to the donor/acceptor (D/A) interface, polymer backbone orientation, and domain purity) are challenging to control. Therefore, new tools and insights are needed to improve the morphology and performance of OSCs.

Here, we report a hydrocarbon-solvent-based processing system that not only yields higher efficiency single-junction OSCs (PCEs up to 11.7%) than previous halogenated solvent methods, but also offers important morphological insights and new facile methods to control BHJ morphology beyond that achievable using the previous halogenated solvent system. Our hydrocarbon process combines the synergistic effects of a hydrocarbon solvent named 1,2,4-trimethylbenzene (TMB), a novel additive named 1-phenylnaphthalene (PN), an optimal alkyl chain length and pronounced temperature-dependent aggregation of the donor polymer. This advance is facilitated by a series of polymers that exhibit a strong temperature-dependent aggregation property, which enables excellent solubility of the polymers in hydrocarbon solvents at elevated temperatures (>80 °C). The PN additive plays a critical role, as it simultaneously introduces several beneficial changes to the morphological and photovoltaic properties of the cells. The PN additive drives the polymer backbone orientation relative to the substrate from edge-on to face-on, reduces the domain size, and increases the domain purity of the BHJ films, hence leading to a large enhancement of the PCE from 6.4% to 11.7%. The host solvent, TMB, is also important, as it enables a better molecular orientation relative to the polymer:fullerene interfaces than is found in films processed from halogenated solvents. Our studies also provide important insights into the critical influences of a small difference in the polymer alkyl chain length on the blend morphology of OSCs. On the one hand, increasing the length of alkyl chains results in a beneficial change: the polymer backbone orientation gradually turns from edge-on to face-on relative to the electrodes. On the other hand, longer alkyl chains, especially $C_{10}C_{14}$, are found to be detrimental to the domain size and domain purity. The balancing of these two anti-synergistic effects led to an optimized choice of alkyl chain (C_9C_{13}) for the processing system of TMB with PN (TMB–PN). In comparison, the optimized alkyl chain length is different for the processing system of CB with

[1]Department of Chemistry and Energy Institute, The Hong Kong University of Science and Technology, Clear Water Bay, Kowloon, Hong Kong. [2]State Key Laboratory for Mechanical Behavior of Materials, Xi'an Jiaotong University, Xi'an 710049, China. [3]HKUST-Shenzhen Research Institute, No. 9 Yuexing 1st Road, Hi-tech Park, Nanshan, Shenzhen 518057, China. [4]Department of Physics, North Carolina State University, Raleigh, North Carolina 27695, USA. †These authors contributed equally to this work. *e-mail: msewma@mail.xjtu.edu.cn; hyan@ust.hk

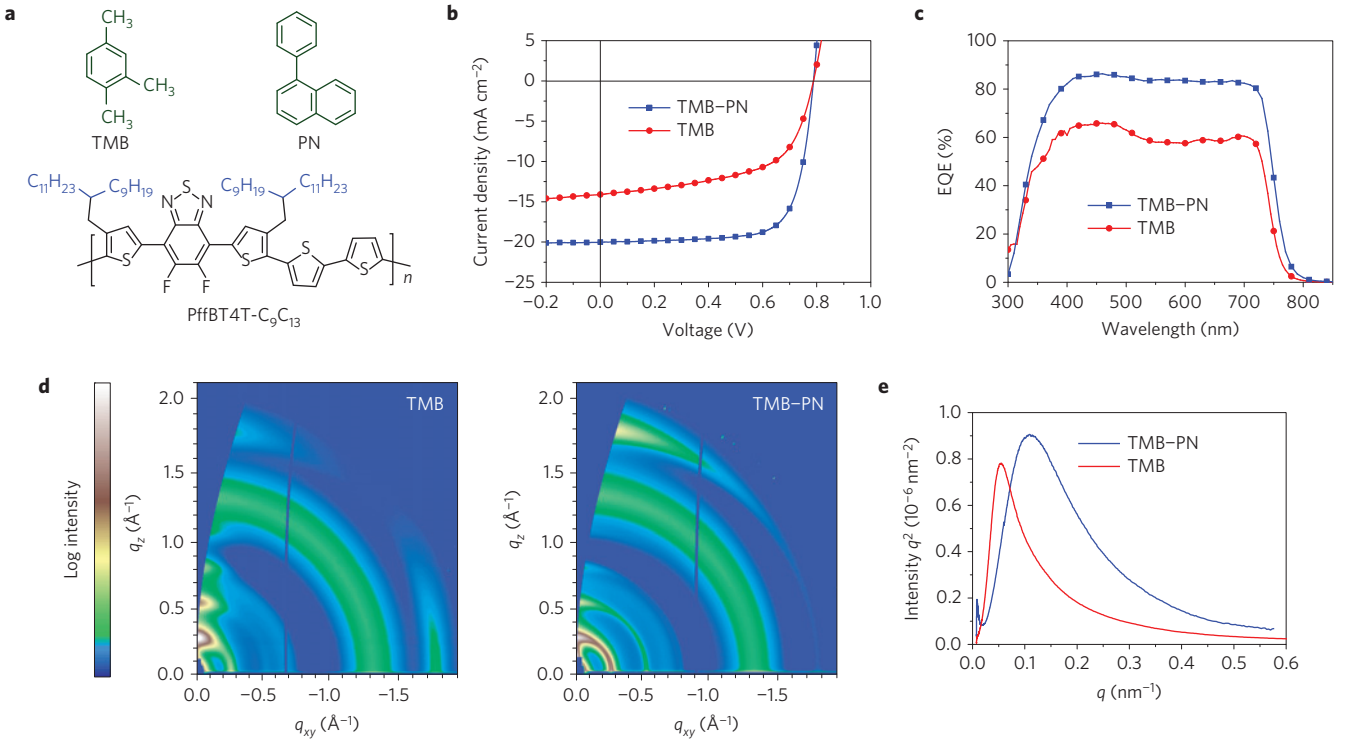

Figure 1 | Chemical structures and characterizations. a, Chemical structures of TMB, PN and PffBT4T-C_9C_{13}. **b**–**e**, *J*–*V* (**b**), EQE curves (**c**), two-dimensional GIWAXS images (**d**) and RSoXS plots (**e**) of PffBT4T-C_9C_{13}:$PC_{71}BM$-based films processed from TMB or TMB–PN. The relative domain purity is 0.74 for TMB compared to 1.00 for TMB–PN.

Table 1 | Solar cell and RSoXS characteristics of PffBT4T-C_9C_{13}:$PC_{71}BM$ processed from different solvents.

	V_{OC} (mV)	J_{sc} (mA cm^{-2})	FF (%)	PCE (%)	Domain spacing (nm)	Domain purity	Anisotropy parameter
TMB–PN	784 ± 4	19.8 ± 0.4	73 ± 1	11.3 ± 0.1 (11.7)	38	1.00	0.26
TMB	773 ± 14	13.2 ± 1.4	55 ± 4	5.6 ± 0.5 (6.4)	56	0.74	0.29
CB–DIO	767 ± 6	18.3 ± 0.5	66 ± 2	9.3 ± 0.1 (9.6)	40	0.90	0.14

The values in the parentheses are from the best devices. The statistics are from 50 devices.

DIO (CB–DIO). This provides important guidelines for developing high-performance OSCs based on environmentally friendly solvent systems from matched polymers.

Morphology and performance

The selection of TMB (Fig. 1a) as the host solvent is due to its high boiling point (to disaggregate and dissolve donor polymers at elevated temperatures) and excellent solubility for fullerenes[24]. On the other hand, the most important challenge is the selection of a hydrocarbon additive that must meet several stringent requirements in order for the OSCs to perform well. First, the additive needs to have a high boiling point, which is crucial to achieve an optimal BHJ morphology[25]. For example, the state-of-the-art DIO additive has a boiling point of 332 °C. Second, the additive should also be a poor solvent for the polymer but a good solvent for fullerenes[25]. For this reason, aliphatic hydrocarbons are ruled out because they are poor solvents for fullerenes. Among the aromatic hydrocarbons, those with sufficiently high boiling points typically exhibit melting points significantly higher than room temperature, and thus cannot be used as liquid additives. Among commercially available hydrocarbons, the only qualified option for an additive we found is PN (Fig. 1a). Owing to its highly twisted molecular structure (Supplementary Fig. 1), the PN additive exhibits a suitably high boiling point (325 °C) yet maintains a particularly low melting point, allowing it to be used as a liquid additive. In contrast, an isomer of PN (2-phenylnaphthalene), which has a less twisted structure than that of PN itself, has a high melting point of 103 °C. The physical properties of PN and several disqualified hydrocarbon additives are shown in Supplementary Table 1. Last, it was found that PN is indeed an outstanding solvent for fullerenes[26] but a poor solvent for our donor polymers even at elevated temperatures.

Bulk-heterojunction OSCs were fabricated with the architecture of ITO/ZnO/polymer:$PC_{71}BM$/V_2O_5/Al. The best polymer used here is poly[(5,6-difluoro-2,1,3-benzothiadiazol-4,7-diyl)-*alt*-(3,3‴- di(2-nonyltridecyl)-2,2′;5′,2″;5″,2‴-quaterthiophen-5,5‴-diyl)] (PffBT4T-C_9C_{13}, Fig. 1a). The reason for using this polymer will be discussed later. The blend films were spin-cast from warm TMB–PN solutions to make use of the temperature-dependent aggregation property[10] of the donor polymer (Supplementary Fig. 2). OSC efficiencies up to 11.7% were achieved under air mass 1.5 global (AM1.5G) one-sun illuminations (Fig. 1b,c and Table 1), outperforming the previous best OSCs processed from toxic halogenated solvents[10]. The integrated current from the external quantum efficiency (EQE) spectrum is 19.9 mA cm^{-2}, which is consistent with the current obtained from the *J*–*V* measurement. One of the high-performance devices was certified at an accredited laboratory, confirming a PCE of 11.5% (Supplementary Fig. 3). On the other hand, the solar cells processed from TMB without the PN additive showed a much poorer performance of 6.4% (Fig. 1b,c

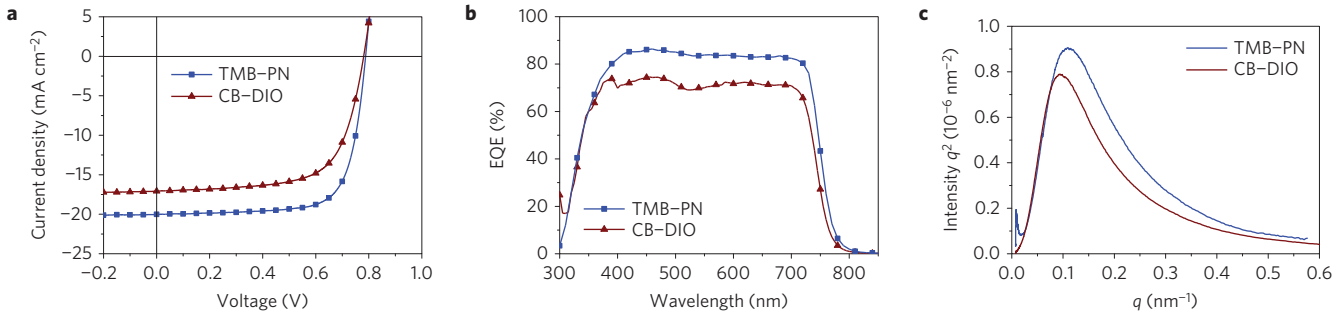

Figure 2 | Characterization of PffBT4T-C_9C_{13}:$PC_{71}BM$ processed from CB–DIO and TMB–PN. a, *J*–*V* curves of the corresponding solar cells. **b**, EQE spectra of the cells. **c**, RSoXS plots of the blend films. The relative domain purity is 0.90 for CB–DIO compared to 1.00 for TMB–PN.

and Table 1), highlighting the marked impact of the PN additive on OSC performance.

The influences of PN on the morphological and photovoltaic properties of the OSCs were studied by a combination of techniques, including grazing-incidence wide-angle X-ray scattering (GIWAXS), resonant soft X-ray scattering (RSoXS) and atomic force microscopy (AFM). First, GIWAXS data for the blend films processed from TMB or TMB–PN both showed high polymer crystallinity (Fig. 1d), with strong lamellar (100), (200), (300) and even (400) reflection peaks and (010) peaks clearly visible. In addition, both blend films exhibit a bimodal texture with both edge-on and face-on populations. The (010) π−π stacking and the lamellar reflections have peaks in the in-plane and out-of-plane directions. For the blend film processed from TMB, the (010) π−π reflection peak is mainly located in the in-plane direction and the lamellar peaks in the out-of-plane direction, indicating a more 'edge-on' polymer backbone orientation relative to the substrate. In contrast, the films processed from TMB–PN exhibit a significant (010) π−π stacking peak in the out-of-plane direction, with a corresponding increase in lamellar peak intensity in the in-plane direction. This suggests that the polymer texture is switched from a preferred 'edge-on' to a preferred 'face-on' owing to the addition of PN. Second, RSoXS (refs 27,28) and AFM revealed that the film processed from TMB shows a larger median (centre-to-centre) spacing of polymer-rich domains of 56 nm than that processed from TMB–PN, which at 38 nm is a near-ideal length scale of phase separation for the BHJ OSCs (Table 1, Fig. 1e and Supplementary Fig. 4)[29,30]. In addition, the average composition variation, that is, average relative purity of all domains of the blend film processed from TMB–PN is much higher (1.00) than that of films processed from TMB (0.74). It has been shown that a high average domain purity is critical to suppress charge carrier recombination and improve overall device performance[31–33]. It is clear that the addition of PN improved the device performance by simultaneously reducing the domain size, increasing the average purity of the domains and promoting the face-on orientation of the polymer backbone relative to the electrode interface.

To further understand the effects of the PN additive, the hole and electron mobilities of the blend films processed from TMB or TMB–PN were measured using the space-charge limited current (SCLC) method (Supplementary Table 2 and Supplementary Fig. 5). It is found that the hole mobilities are similar for the two blends ($\sim 7 \times 10^{-3}$ cm^2 V^{-1} s^{-1}), but the electron mobility is significantly higher for the blend processed from TMB–PN (3.4×10^{-3} cm^2 V^{-1} s^{-1} versus 1.2×10^{-4} cm^2 V^{-1} s^{-1}). A higher and more balanced electron mobility should be an important reason for the higher fill factors of the TMB–PN processed devices. Importantly, the high electron mobility of the blend film processed from TMB–PN is supported by GIWAXS results, which show that the use of PN significantly enhances the aggregation of $PC_{71}BM$ in the blend film. In the GIWAXS two-dimensional maps shown in Fig. 1, the isotropic peak at $q \approx 1.33$ Å corresponds to the $PC_{71}BM$ aggregates. The coherence length of this $PC_{71}BM$ peak is estimated to be about 6.2 nm for the blend film processed from TMB–PN, which is significantly longer than that (4.7 nm) of the film processed from TMB. The higher $PC_{71}BM$ aggregation/crystallinity of the TMB–PN processed film is also consistent with the higher domain purity of the film revealed by the RSoXS data. This means that the polymer and $PC_{71}BM$ is better mixed in the film processed from TMB, whereas the use of the PN additive creates a larger volume fraction of pure $PC_{71}BM$ domain and thus increases the likelihood of the pure $PC_{71}BM$ domain being connected, in turn contributing to increased crystallinity and electron mobility. The reason why PN improves the domain purity may be that it is a poor solvent for the polymer but a good solvent for fullerene[26]. During the warm spin-coating process, as the host solvent TMB evaporates, the volume percentage of PN additive increases. As a result, the polymer starts to pre-aggregate in solution, which allows $PC_{71}BM$ to form purer domains, leading to a higher crystallinity and electron mobility. A similar self-consistent strong correlation of domain purity, electron mobility and $PC_{71}BM$ aggregation/crystallinity was also reported recently[34].

The differences between the environmentally friendly processing procedure based on TMB–PN and the conventional system of CB–DIO were also studied. The device using PffBT4T-C_9C_{13} as the donor polymer and processed from CB–DIO showed an inferior performance of 9.4%, mainly as a result of the lower J_{SC} and fill factor (FF) (Table 1 and Fig. 2a,b). GIWAXS and RSoXS data revealed that the two films processed from TMB–PN or CB–DIO both exhibit high polymer crystallinity and small domain sizes (Fig. 3c,f and Table 1 and Fig. 2c). However, the relative average purity of all domains for the film processed from CB–DIO is lower (90%) than that for TMB–PN (Table 1). Moreover, polarized soft X-ray scattering (PSoXS) was used to probe the molecular orientation relative to D/A interfaces via scattering anisotropy[35,36]. The anisotropy parameter obtained for the film processed from TMB–PN is 0.26, which is significantly higher than that (0.14) for CB–DIO (Table 1 and Supplementary Fig. 6). This indicates that the film processed from TMB–PN exhibits a more face-on molecular orientation[36] relative to polymer:fullerene interfaces. Note that the film processed from TMB without PN additive also exhibits an excellent molecular orientation (anisotropy parameter 0.29) (Table 1 and Supplementary Fig. 6), which indicates that the better molecular orientation of TMB–PN than CB–DIO is attributed to TMB rather than PN. A better molecular orientation and higher domain purity have been shown to be crucial for efficient charge generation and minimized recombination, respectively[31–33,36], which can help explain the excellent performance achieved in this work. The superiority of the environmentally friendly process over conventional halogenated solvents is also maintained relative to the best polymer halogenated solvent match, which yields a lower PCE for an identical optical band gap (Supplementary Fig. 7)[10].

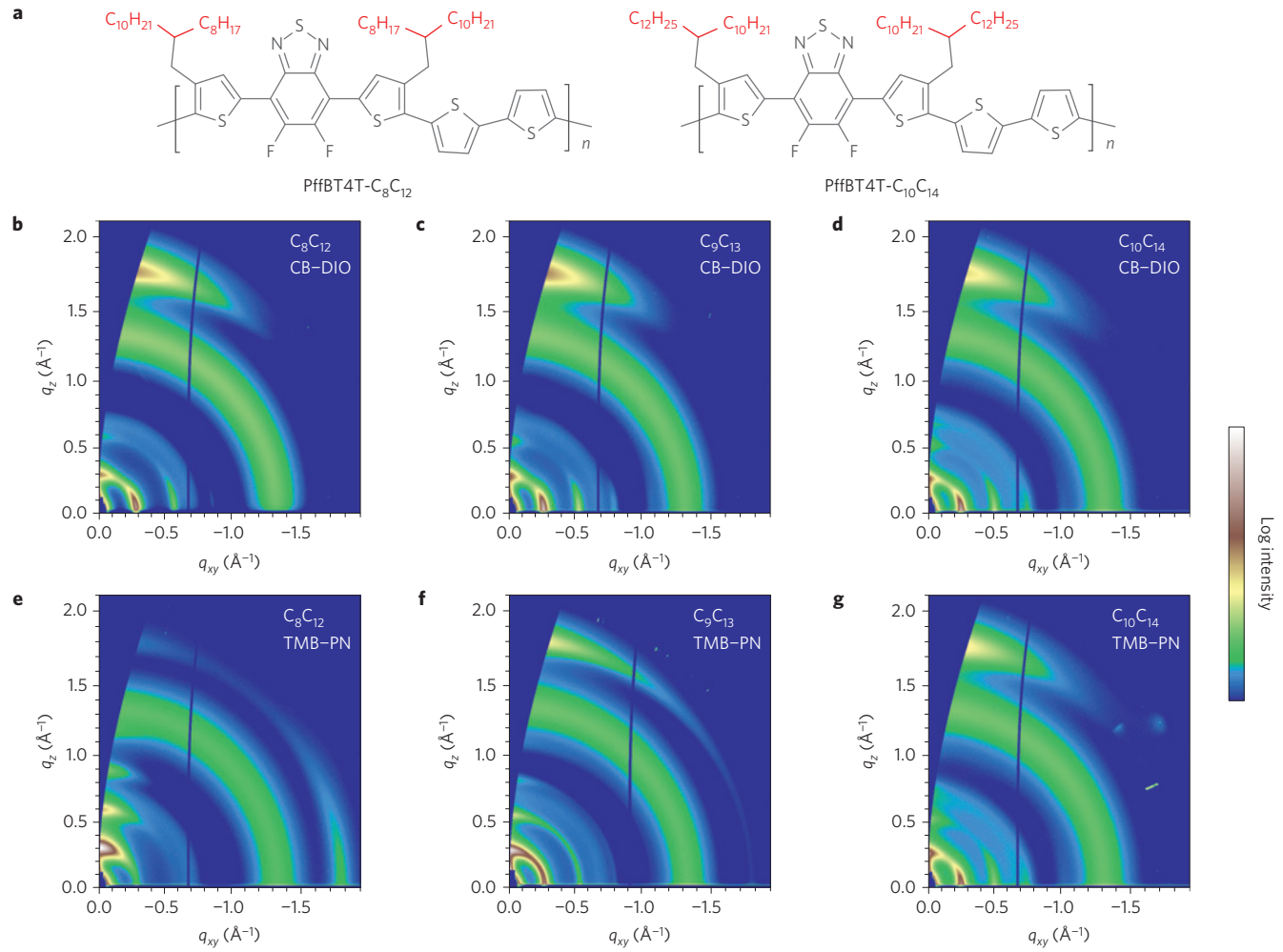

Figure 3 | The influence of alkyl chain lengths on polymer texture. a, Chemical structures of PffBT4T-C_8C_{12} and PffBT4T-$C_{10}C_{14}$. **b–d**, Two-dimensional GIWAXS images of PffBT4T-C_8C_{12}:$PC_{71}BM$ (**b**), PffBT4T-C_9C_{13}:$PC_{71}BM$ (**c**) and PffBT4T-$C_{10}C_{14}$:$PC_{71}BM$ (**d**) blend films processed from CB–DIO. **e–g**, Two-dimensional GIWAXS images of PffBT4T-C_8C_{12}:$PC_{71}BM$ (**e**), PffBT4T-C_9C_{13}:$PC_{71}BM$ (**f**) and PffBT4T-$C_{10}C_{14}$:$PC_{71}BM$ (**g**) blend films processed from TMB–PN.

Table 2 | Solar cell performance of polymers with different alkyl chains processed from different solvents.

Polymer	Processing solvents	V_{OC} (mV)	J_{sc} (mA cm^{-2})	FF (%)	PCE (%)
PffBT4T-C_8C_{12}	CB–DIO	774 ± 3	18.8 ± 0.2	69 ± 1	10.0 ± 0.2
PffBT4T-C_9C_{13}	CB–DIO	767 ± 6	18.3 ± 0.5	66 ± 2	9.3 ± 0.1
PffBT4T-$C_{10}C_{14}$	CB–DIO	779 ± 3	16.4 ± 0.2	70 ± 1	8.9 ± 0.1
PffBT4T-C_8C_{12}	TMB–PN	783 ± 4	17.0 ± 1.0	69 ± 3	9.2 ± 0.3
PffBT4T-C_9C_{13}	TMB–PN	784 ± 4	19.8 ± 0.4	73 ± 1	11.3 ± 0.1
PffBT4T-$C_{10}C_{14}$	TMB–PN	781 ± 5	17.8 ± 0.4	74 ± 1	10.3 ± 0.2

In all cases, the fullerene used is $PC_{71}BM$. The statistics are from 50 devices for PffBT4T-C_9C_{13} and 5 devices for others.

The excellent morphology of the TMB–PN-processed films enables the use of thick active layers (350–400 nm), which enhances light harvesting and thus improves the J_{SC} of the devices.

The role of alkyl chains

To study the influence of the polymer alkyl chain length on morphology and device performance, solar cell devices with PffBT4T-C_8C_{12}, PffBT4T-C_9C_{13} or PffBT4T-$C_{10}C_{14}$ (Fig. 3a) as donor polymers processed from TMB–PN or CB–DIO were fabricated and the morphology differences were investigated. It was found that when processed from CB–DIO, the average device efficiency decreases from 10.0% to 9.3%, and then to 8.9% with increasing alkyl chain length (Table 2 and Supplementary Fig. 8). When TMB–PN was used as the processing solvent, the trend of PCE among the three polymers is different, with the average PCE increasing from 9.2% to 11.3%, then decreasing to 10.3% with increasing alkyl chain length (Table 2 and Supplementary Fig. 9). First, GIWAXS results revealed the impacts of alkyl chain length on the orientation of the polymer backbone. For the CB–DIO-based processing system all the three polymers exhibit similar face-on polymer backbone orientation, with the strong (010) π–π stacking peaks in the out-of-plane direction and (*h*00) peaks in the in-plane direction (Fig. 3b–d). For the films processed from TMB–PN,

Table 3 | RSoXS characteristics of polymers with different alkyl chains processed from TMB–PN.

Polymer	Domain spacing (nm)	Domain purity
PffBT4T-C_8C_{12}	34	1.04
PffBT4T-C_9C_{13}	38	1.00
PffBT4T-$C_{10}C_{14}$	56	0.88

In all cases, the fullerene used is $PC_{71}BM$.

however, the polymer texture is significantly different for the three polymers (Fig. 3e–g). Whereas the (010) π−π stacking peak is predominantly located in the in-plane direction for PffBT4T-C_8C_{12}, the relative intensities of the (010) π−π stacking peaks increase significantly in the out-of-plane direction for PffBT4T-C_9C_{13} and PffBT4T-$C_{10}C_{14}$, demonstrating that the face-on orientation becomes more pronounced with longer alkyl chains. On the other hand, RSoXS revealed that the median domain spacing (38 nm) of PffBT4T-C_9C_{13}-based blend film is fairly comparable to that of PffBT4T-C_8C_{12} (34 nm) (Table 3 and Supplementary Fig. 10), and the domain purity of PffBT4T-C_9C_{13} is also similar to that of PffBT4T-C_8C_{12} (relative purity is 1.00 versus 1.04). However, when the alkyl chain length was increased to $C_{10}C_{14}$, the domain spacing increased significantly to 56 nm, whereas the relative domain purity decreased to 0.88 (Table 3 and Supplementary Fig. 10). By balancing these two anti-synergistic effects of alkyl chains on polymer backbone orientation and domain size/purity, C_9C_{13} is shown to be the optimal choice of alkyl chain for the TMB–PN-based processing system, as it can achieve a face-on orientation, a small domain size and a high domain purity simultaneously.

To explore the influence of the alkyl chain length on the polymer backbone orientation for the CB–DIO system in a broader survey, two polymers with even shorter alkyl chains were synthesized and the blend films based on them were characterized by GIWAXS (Supplementary Fig. 11). It was found that the polymer texture also gradually turns to edge-on when even shorter alkyl chains were used in conjunction with the CB–DIO solvent system. It is thus clear that, in both processing systems, shorter alkyl chains tend to promote edge-on orientation whereas longer alkyl chains change the polymer texture from edge-on to face-on. The difference between the two processing systems is that the minimal length of the alkyl chain to drive the polymer texture from edge-on to face-on is longer for the TMB–PN processing system than for the CB–DIO system. These findings offer insights into why the optimized alkyl chain lengths in the two processing systems are different. Environmentally friendly processing from hydrocarbon solvents thus requires optimization of its own side-chain design and the processing of active layers needs to be considered a synergistic whole.

Scope of the processing system

To explore the applicable scope of the TMB–PN processing system, solar cell devices based on a large-bandgap polymer, namely PffT2-FTAZ-$C_{10}C_{14}$ and $PC_{71}BM$, were fabricated (structure shown in Supplementary Fig. 12)[37]. The polymer features a similar temperature-dependent aggregation property and the films were cast from warm TMB–PN solutions. An excellent PCE of 8.7% was achieved from thick-film devices, which outperformed the corresponding devices processed from CB–DIO (7.7%) and is among the best results yet reported for large-bandgap polymers (~1.9 eV, Supplementary Table 3 and Supplementary Fig. 13). More importantly, RSoXS and PSoXS measurements were performed to investigate the morphology difference between two films processed from CB–DIO or TMB–PN for PffT2-FTAZ-$C_{10}C_{14}$. The results reveal that the film processed from TMB–PN has a higher domain purity, better molecular orientation and a slightly smaller domain size than that from CB–DIO (Supplementary Fig. 14 and Supplementary Table 4). These are exactly the same advantageous features of TMB–PN over CB–DIO for the PffBT4T-C_9C_{13}-based system. It is thus clear that the TMB–PN processing system is also effective for other polymers with similar temperature-dependent aggregation properties. In addition, two other well-known polymers (PTB7 and PTB7-Th, structures shown in Supplementary Fig. 12) were also used to test the applicable scope of the TMB–PN processing system. Whereas PTB7-based cells processed from TMB–PN led to an enhanced efficiency (8.4%) over the control device processed from CB–DIO (7.9%), PTB7-Th-based devices processed from TMB–PN showed comparable performances to the control devices (Supplementary Figs 15 and 16 and Supplementary Table 5). Note that the efficiencies of our PTB7 or PTB7-Th control devices are comparable to the reported control devices without special interlayers or device engineering[38–41]. The promising results achieved by using TMB–PN clearly support the wide-ranging applicability of the new solvent system, and will inspire the community to develop further hydrocarbon solvent systems.

Conclusion

In summary, a hydrocarbon solvents-based processing system was demonstrated and yielded even better OSC morphology and performance than that obtainable with conventional halogenated solvents. Our results offer a new avenue to optimize several important aspects of the OSC morphology. The PN additive was found to play a critical role by introducing multiple beneficial effects (promoting face-on polymer backbone orientation, reducing domain size, and increasing domain purity) and thus enhancing the PCE of the OSCs from 6.4% to 11.7%. The choice of the host solvent TMB was also important, as it improves the molecular orientation relative to the D/A interfaces in the BHJ film. Our study also revealed the marked morphology effects introduced by a small change in the alkyl chain length, which enabled a rational selection of the alkyl chain length and the subsequent achievemnt of the best morphology and OSC performance. Our novel solvent processing system requires no excessive chemical synthesis or new device engineering, and is readily applicable to other material systems. Our study thus offers a simple yet effective approach towards highly efficient and environmentally friendly OSCs.

Methods

Solar cell fabrication and testing. Pre-patterned ITO-coated glass with a sheet resistance of ~15 Ω/□ was used as the substrate. It was cleaned by sequential ultrasonication in soap deionized water, deionized water, acetone and isopropanol for 15 min at each step. The washed substrates were further treated with an ultraviolet O_3 cleaner (Novascan, PSD Series digital ultraviolet ozone system) for 30 min. A topcoat layer of ZnO (a diethylzinc solution, 15 wt% in toluene, diluted with tetrahydrofuran) was spin-coated onto the ITO substrate at a spinning rate of 5,000 r.p.m. for 30 s and then baked in air at 150 °C for 20 min. Active layer solutions (polymer:fullerene weight ratio 1:1.2) were prepared in TMB or CB with or without 2.5% of PN or DIO. The polymer concentration is 6 mg ml^{-1} for PffBT4T-C_8C_{12}, 10 mg ml^{-1} for PffBT4T-C_9C_{13}, 18 mg ml^{-1} for PffBT4T-$C_{10}C_{14}$ and 10 mg ml^{-1} for PffT2-FTAZ-$C_{10}C_{14}$. To completely dissolve the polymer, the active layer solution should be stirred on a hot plate at 100 °C for at least 1 h. Before spin coating, both the polymer solution and ITO substrate are preheated on a hot plate at 100 °C. Active layers were spin-coated from the warm polymer solution on the preheated substrate in a N_2 glovebox at 600 r.p.m. For PTB7 and PTB7-Th, the films were spin-coated at room temperature at 2,000 r.p.m. from 16 mg ml^{-1} and 10 mg ml^{-1} solutions, respectively. The optimal PffBT4T-C_9C_{13}:$PC_{71}BM$ film thickness is 350–400 nm. The active layers were then treated with vacuum to remove the high-boiling-point additives[11]. The blend films were annealed at 80 °C for 5 min before being transferred to the vacuum chamber of a thermal evaporator inside the same glovebox. The residual additive in the active layer was characterized by gas chromatography mass spectrometry (GC-MS) to be negligible (Supplementary Fig. 17). At a vacuum level of 3×10^{-6} torr, a thin layer (20 nm) of V_2O_5 was deposited as the anode interlayer, followed by deposition of 100 nm of Al as the top electrode. All cells were encapsulated using epoxy inside the glovebox. Device J–V characteristics were measured under AM1.5G (100 mW cm^{-2}) using a Newport Class A solar

simulator (94021A, a Xenon lamp with an AM1.5G filter) in air at room temperature. A standard Si diode with KG5 filter was purchased from PV Measurements and calibrated by Newport Corporation. The light intensity was calibrated using the Si diode as a reference cell to bring the spectral mismatch to unity. J–V characteristics were recorded using a Keithley 2400 source meter unit. Typical cells have device areas of 5.9 mm^2, which are defined by a metal mask with an aperture aligned with the device area. EQEs were characterized using a Newport EQE system equipped with a standard Si diode. Monochromatic light was generated from a Newport 300 W lamp source. The EQE of the best cell was measured by Enli Technology. One of our best cells was sent to an accredited solar cell calibration laboratory (Newport) for certification, confirming an efficiency of 11.48 ± 0.25%, with V_{OC} = 0.7907 ± 0.0110 V, I_{SC} = 0.000847 ± 0.000016 A, Area = 0.0429 ± 0.0002 cm^2, FF = 73.5 ± 1.1 (Supplementary Fig. 3).

GIWAXS characterization. GIWAXS measurements were performed at beamline 7.3.3 at the Advanced Light Source[42]. Samples were prepared on Si substrates using blend solutions identical to those used in devices. The 10 keV X-ray beam was incident at a grazing angle of 0.13°–0.17°, which maximized the scattering intensity from the samples. The scattered X-rays were detected using a Dectris Pilatus 2M photon counting detector. The coherence length of $PC_{71}BM$ was calculated from circular averaged profiles by Scherrer analysis[43]:

$$L_c = \frac{2\pi K}{\Delta_q}$$

where Δ_q is the full-width at half-maximum of the peak and K is a shape factor (0.9 was used here).

RSoXS and PSoXS characterization. RSoXS and PSoXS transmission measurements were performed at beamline 11.0.1.2 at the Advanced Light Source[44]. Samples for RSoXS and PSoXS measurements were prepared on a poly(sodium 4-styrenesulfonate)-modified Si substrate under the same conditions as those used for device fabrication, and then transferred by floating in water to a 1.5 mm × 1.5 mm, 100-nm-thick Si_3N_4 membrane supported by a 5 mm × 5 mm, 200-μm-thick Si frame (Norcada). Two-dimensional scattering patterns were collected on an in-vacuum charge-coupled device (CCD) camera (Princeton Instrument PI-MTE). The sample–detector distance was calibrated from the diffraction peaks of a triblock copolymer poly(isoprene-b-styrene-b-2-vinyl pyridine), which has a known spacing of 391 Å. The beam size at the sample is approximately 100 μm by 200 μm. The photon energy was selected to be 284.2 eV owing to high polymer:fullerene contrast. The median domain spacing is calculated from $2\pi/q$, where q here corresponds to half the total scattering intensity (TSI; ref. 36). For a three-phase morphology with equal volume fractions and the mixed polymer:fullerene domains symmetrically distributed between the pure crystalline polymer phase and nearly pure PCBM aggregate phase, the spacing would translate into domains about one-third in size. The composition variation (or relative purity of all domains) over the length scales sampled can be extracted by integrating scattering profiles to yield the integrated sector intensities (ISI). The purer the average domains are, the higher the ISI. The scattering anisotropy parameter was defined as the difference of sector (±10° is used here) scattering intensity perpendicular and parallel to the electric field direction over their sum, which is calculated from PSoXS at 285.2 eV:

$$\mathrm{ISI}_{(\mathrm{vertical,\,horizontal})} = \int I_{\mathrm{avg(vertical,\,horizontal)}}\, q^2(q)\mathrm{d}q$$

$$A(E) \equiv \frac{\mathrm{ISI}_{\mathrm{vertical}} - \mathrm{ISI}_{\mathrm{horizontal}}}{\mathrm{ISI}_{\mathrm{vertical}} + \mathrm{ISI}_{\mathrm{horizontal}}}$$

Synthesis of PffBT4T-C_9C_{13}. The detailed synthesis route can be found in the Supplementary Methods. The NMR data of all the new compounds are included as Supplementary Figs 17–42.

Received 15 August 2015; accepted 16 December 2015; published 25 January 2016

References

1. Yu, G., Gao, J., Hummelen, J. C., Wudl, F. & Heeger, A. J. Polymer photovoltaic cells-enhanced efficiencies via a network of internal donor–acceptor heterojunctions. *Science* **270**, 1789–1791 (1995).
2. Li, G. *et al.* High-efficiency solution processable polymer photovoltaic cells by self-organization of polymer blends. *Nature Mater.* **4**, 864–868 (2005).
3. Kim, J. Y. *et al.* Efficient tandem polymer solar cells fabricated by all-solution processing. *Science* **317**, 222–225 (2007).
4. Peet, J. *et al.* Efficiency enhancement in low-bandgap polymer solar cells by processing with alkane dithiols. *Nature Mater.* **6**, 497–500 (2007).
5. Chen, H.-Y. *et al.* Polymer solar cells with enhanced open-circuit voltage and efficiency. *Nature Photon.* **3**, 649–653 (2009).
6. Park, S. H. *et al.* Bulk heterojunction solar cells with internal quantum efficiency approaching 100%. *Nature Photon.* **3**, 297–302 (2009).
7. He, Z. *et al.* Enhanced power-conversion efficiency in polymer solar cells using an inverted device structure. *Nature Photon.* **6**, 591–595 (2012).
8. Guo, X. *et al.* Polymer solar cells with enhanced fill factors. *Nature Photon.* **7**, 825–833 (2013).
9. Heeger, A. J. 25th anniversary article: bulk heterojunction solar cells: understanding the mechanism of operation. *Adv. Mater.* **26**, 10–28 (2014).
10. Liu, Y. *et al.* Aggregation and morphology control enables multiple cases of high-efficiency polymer solar cells. *Nature Commun.* **5**, 5293 (2014).
11. He, Z. *et al.* Single-junction polymer solar cells with high efficiency and photovoltage. *Nature Photon.* **9**, 174–179 (2015).
12. You, J. *et al.* A polymer tandem solar cell with 10.6% power conversion efficiency. *Nature Commun.* **4**, 1446 (2013).
13. Zhou, H. *et al.* Polymer homo-tandem solar cells with best efficiency of 11.3%. *Adv. Mater.* **27**, 1767–1773 (2015).
14. Yusoff, A. R. b. M. *et al.* A high efficiency solution processed polymer inverted triple-junction solar cell exhibiting a power conversion efficiency of 11.83%. *Energy Environ. Sci.* **8**, 303–316 (2015).
15. Shaheen, S. E. *et al.* 2.5% efficient organic plastic solar cells. *Appl. Phys. Lett.* **78**, 841–843 (2001).
16. Chueh, C.-C. *et al.* Non-halogenated solvents for environmentally friendly processing of high-performance bulk-heterojunction polymer solar cells. *Energy Environ. Sci.* **6**, 3241–3248 (2013).
17. Chen, X., Liu, X., Burgers, M. A., Huang, Y. & Bazan, G. C. Green-solvent-processed molecular solar cells. *Angew. Chem. Int. Ed.* **53**, 14378–14381 (2014).
18. Guo, X., Zhang, M., Cui, C., Hou, J. & Li, Y. Efficient polymer solar cells based on poly(3-hexylthiophene) and indene–C60 bisadduct fabricated with non-halogenated solvents. *ACS Appl. Mater. Interfaces* **6**, 8190–8198 (2014).
19. Synooka, O., Eberhardt, K. R. & Hoppe, H. Chlorine-free processed high performance organic solar cells. *RSC Adv.* **4**, 16681–16685 (2014).
20. Deng, Y. *et al.* Low bandgap conjugated polymers based on mono-fluorinated isoindigo for efficient bulk heterojunction polymer solar cells processed with non-chlorinated solvents. *Energy Environ. Sci.* **8**, 585–591 (2015).
21. Sprau, C. *et al.* Highly efficient polymer solar cells cast from non-halogenated xylene/anisaldehyde solution. *Energy Environ. Sci.* **8**, 2744–2752 (2015).
22. Zhao, W., Ye, L., Zhang, S., Sun, M. & Hou, J. A universal halogen-free solvent system for highly efficient polymer solar cells. *J. Mater. Chem. A* **3**, 12723–12729 (2015).
23. Huang, Y., Kramer, E. J., Heeger, A. J. & Bazan, G. C. Bulk heterojunction solar cells: morphology and performance relationships. *Chem. Rev.* **114**, 7006–7043 (2014).
24. Scrivens, W. A. & Tour, J. M. Potent solvents for C60 and their utility for the rapid acquisition of 13C NMR data for fullerenes. *J. Chem. Soc. Chem. Commun.* 1207–1209 (1993).
25. Lee, J. K. *et al.* Processing additives for improved efficiency from bulk heterojunction solar cells. *J. Am. Chem. Soc.* **130**, 3619–3623 (2008).
26. Ruoff, R. S., Tse, D. S., Malhotra, R. & Lorents, D. C. Solubility of fullerene (C60) in a variety of solvents. *J. Phys. Chem.* **97**, 3379–3383 (1993).
27. Swaraj, S. *et al.* Nanomorphology of bulk heterojunction photovoltaic thin films probed with resonant soft X-ray scattering. *Nano Lett.* **10**, 2863–2869 (2010).
28. Collins, B. A. *et al.* Absolute measurement of domain composition and nanoscale size distribution explains performance in PTB7:PC71BM solar cells. *Adv. Energy Mater.* **3**, 65–74 (2013).
29. Chen, W. *et al.* Hierarchical nanomorphologies promote exciton dissociation in polymer/fullerene bulk heterojunction solar cells. *Nano Lett.* **11**, 3707–3713 (2011).
30. Shaw, P. E., Ruseckas, A. & Samuel, I. D. W. Exciton diffusion measurements in poly(3-hexylthiophene). *Adv. Mater.* **20**, 3516–3520 (2008).
31. Stuart, A. C. *et al.* Fluorine substituents reduce charge recombination and drive structure and morphology development in polymer solar cells. *J. Am. Chem. Soc.* **135**, 1806–1815 (2013).
32. Albrecht, S. *et al.* Quantifying charge extraction in organic solar cells: the case of fluorinated PCPDTBT. *J. Phys. Chem. Lett.* **5**, 1131–1138 (2014).
33. Ma, W. *et al.* Domain purity, miscibility, and molecular orientation at donor/acceptor interfaces in high performance organic solar cells: paths to further improvement. *Adv. Energy Mater.* **3**, 864–872 (2013).
34. Mukherjee, S. *et al.* Importance of domain purity and molecular packing in efficient solution-processed small-molecule solar cells. *Adv. Mater.* **27**, 1105–1111 (2015).
35. Collins, B. A. *et al.* Polarized X-ray scattering reveals non-crystalline orientational ordering in organic films. *Nature Mater.* **11**, 536–543 (2012).
36. Tumbleston, J. R. *et al.* The influence of molecular orientation on organic bulk heterojunction solar cells. *Nature Photon.* **8**, 385–391 (2014).

37. Li, Z. *et al.* Dramatic performance enhancement for large bandgap thick-film polymer solar cells introduced by a difluorinated donor unit. *Nano Energy* **15**, 607–615 (2015).
38. Ouyang, X., Peng, R., Ai, L., Zhang, X. & Ge, Z. Efficient polymer solar cells employing a non-conjugated small-molecule electrolyte. *Nature Photon.* **9**, 520–524 (2015).
39. Lu, L., Xu, T., Chen, W., Landry, E. S. & Yu, L. Ternary blend polymer solar cells with enhanced power conversion efficiency. *Nature Photon.* **8**, 716–722 (2014).
40. Nian, L. *et al.* Photoconductive cathode interlayer for highly efficient inverted polymer solar cells. *J. Am. Chem. Soc.* **137**, 6995–6998 (2015).
41. Liao, S.-H. *et al.* Single junction inverted polymer solar cell reaching power conversion efficiency 10.31% by employing dual-doped zinc oxide nano-film as cathode interlayer. *Sci. Rep.* **4**, 6813 (2014).
42. Hexemer, A. *et al.* A SAXS/WAXS/GISAXS beamline with multilayer monochromator. *J. Phys. Conf. Ser.* **247**, 012007 (2010).
43. Rivnay, J., Noriega, R., Kline, R. J., Salleo, A. & Toney, M. F. Quantitative analysis of lattice disorder and crystallite size in organic semiconductor thin films. *Phys. Rev. B* **84**, 045203 (2011).
44. Gann, E. *et al.* Soft X-ray scattering facility at the Advanced Light Source with real-time data processing and analysis. *Rev. Sci. Instrum.* **83**, 045110 (2012).

Acknowledgements

The work was partially supported by the National Basic Research Program of China (973 Program; 2013CB834705), HK JEBN Limited (Hong Kong), the Hong Kong Research Grants Council (T23–407/13-N, N_HKUST623/13, and 606012), HKUST President's Office through SSTSP scheme (project ref number: EP201) and the National Natural Science Foundation of China (NSFC, #21374090, 21504066, 21534003 and 51320105014). We thank Enli Technology Co., Ltd (Taiwan) for carrying out EQE measurements and Raynergy Tek Incorporation (Taiwan) for providing building blocks. H.A. is supported by ONR grants N000141410531 and N00141512322. X-ray data was acquired at beamlines 11.0.1.2 and 7.3.3 at the Advanced Light Source, which is supported by the Director, Office of Science, Office of Basic Energy Sciences, of the US Department of Energy under Contract No. DE-AC02-05CH11231.

Author contributions

J.Z. selected the solvent/additive and synthesized PffBT4T-C_9C_{13}; Y.L. fabricated and optimized the devices; Y.L. prepared the devices for certification and samples for X-ray characterization; W.M. collected the X-ray data; G.Y. analysed the X-ray data supervised by W.M.; K.J. fabricated and optimized the devices based on PTB7 and PffBT4T-C_8C_{12}; H.L. synthesized PffT2-FTAZ-$C_{10}C_{14}$; J.Z., H.Y., W.M. and H.A. integrated the interpretation and drafted the paper; H.Y. conceived and directed the project; all authors commented on the final paper.

Additional information

Supplementary information is available online. Reprints and permissions information is available online at www.nature.com/reprints. Correspondence and requests for materials should be addressed to W.M. or H.Y.

Competing interests

The authors declare no competing financial interests.